IOP Publishing Journal of Physics A: Mathematical and Theoretical

J. Phys. A: Math. Theor. **53** (2020) 064002 (19pp) https://doi.org/10.1088/1751-8121/ab5e4e

Synchronization in disordered superconducting arrays

Kurt Wiesenfeld

School of Physics, Georgia Institute of Technology, Atlanta, GA, United States of America

E-mail: kurt.wiesenfeld@physics.gatech.edu

Received 9 July 2019, revised 23 November 2019
Accepted for publication 3 December 2019
Published 16 January 2020

Abstract

This paper describes the effect of quenched disorder on the synchronization properties of a class of circuits known as Josephson junction arrays. The methodology extends the 'dynamical systems approach' used to analyze identical-element arrays to a 'statistical mechanics approach' to incorporate disorder, a topic of great importance from the perspective of device applications. The essential step is to map the circuit equations onto a version of the fabled Kuramoto model, whose tractability allows one to quantify the system-wide quality of synchronization.

Keywords: Josephson junction array, synchronization, disorder, Kuramoto model, Sakaguchi

(Some figures may appear in colour only in the online journal)

1. Introduction

The context for this paper is a desired goal in applied physics, namely the creation of a high-quality, tunable, high-frequency voltage source. The device in question uses superconducting circuit elements called Josephson junctions. A single Josephson junction can convert a constant input current into a periodic voltage output, whose frequency varies monotonically with the input current. Typical frequencies can be very high by electronic standards, and can reach levels of one terahertz or more.

A single junction is physically small ($\sim$1 micron), has low impedence ($\sim$1 ohm), and generates low power output ($\sim$10 nanowatts). This motivates building arrays having many junctions, coupled in such a way that the individual elements exactly frequency-lock. In the ideal limit of identical junctions, the problem reduces to finding an architecture and operating regime where the in-phase state is an attractor. A lot of attention has been devoted to this topic, much of it found in the dynamical systems literature.

As a practical matter, however, the inevitable variability in junction properties presents a barrier to creating a useful device. On the plus side, the nonlinear nature of the circuit dynamics makes it possible for perfect frequency locking even for non-identical junctions, provided the disorder is not 'too large'. This begs a series of questions. How much disorder can be tolerated? Is existing fabrication technology good enough to achieve complete locking? If not, what tolerances must be achieved? Finally, what variety of Josephson junction, and what circuit architectures, have the greatest tolerance?

2. Background

2.1. Single junctions and arrays

The term Josephson junction refers to any configuration where two pieces of superconductor are separated by a thin gap. The gap may be a layer of vacuum, insulator, semiconductor, metal, or even another type of superconductor. Although the fundamental physics of the Josephson junction is quantum mechanical [1–4] for the purposes of this paper it can be treated as a nonlinear circuit element [5–7]. A Josephson junction's current-voltage relation is defined by the pair of equations

$$I = \frac{\hbar c}{2e}\ddot{\phi} + \frac{\hbar}{2er}\dot{\phi} + I_c \sin\phi \tag{1}$$

$$V = \frac{\hbar}{2e}\dot{\phi} \tag{2}$$

where I is the current through the junction, and V is the voltage drop across the junction. In equation (1), the three terms on the right represent, respectively, the displacement current, the normal current, and the super-current; the capacitance c, resistance r, and critical current I_c depend on the junction's material composition and geometry; and $\hbar$ is Planck's constant divided by 2π and e is the fundamental electron charge. The quantity ϕ is an angular dynamical variable (equal to the phase difference between the macroscopic wave functions on either side of the junction), and the overdot denotes differentiation with respect to time.

By convention, Josephson junctions are divided into two categories, depending on whether or not their capacitance is negligible. This distinction has significant physical consequences, and depends on the geometry of the junction. So-called 'point contact' junctions have $c = 0$, while 'tunnel junctions' have $c > 0$.

A Josephson junction can act as a frequency generator because a constant input current can give rise to a periodic output voltage. The frequency can be very high by electronic standards: oscillations of hundreds of gigahertz are common; frequencies up to a terahertz and more have been attained [8]. The disadvantages of single-junctions—low output power and low impedence—can be overcome by building arrays.

2.2. Array architectures

The design of a Josephson junction array allows for considerable flexibility. Individual junctions can be connected to each other is a variety of ways; additional elements can be included in the circuit; external fields can be applied. In this paper, we consider two types of junctions and two different array architectures, representing a total four classes of Josephson arrays. The two junction types are point contact junctions, and tunnel junctions. The two architectures are series arrays, and two dimensional rectangular arrays. In all cases, the array is driven by

a constant bias current and has a generic resistor-inductor-capacitor load. No effects from external fields are considered.

2.3. Kuramoto–Sakaguchi model

In 1975, Kuramoto published a paper describing the onset of spontaneous frequency-locking in a simple model of coupled phase oscillators [9]. Today, this work stands as a theoretical touchstone in the field of emergent behavior, and has spawned a large literature. Of particular interest here is a variation known as the Kuramoto–Sakaguchi model [10]

$$\dot{\theta}_j = \omega_j + \frac{K}{N}\sum_{\ell=1}^{N}\sin\left(\theta_\ell - \theta_j + \alpha\right) \qquad ; \qquad j = 1, 2, \ldots, N \tag{3}$$

where K and α are coupling constants, and the set of bare frequencies ω_j are selected from a given probability distribution $g(\omega)$. K can have either sign, so we can restrict $\alpha \in [-\pi/2, \pi/2]$ without loss of generality. For unimodal g and in the large-N limit, as K is increased from a small value, the system exhibits a transition to partial ordering, i.e. where there first appears a non-zero fraction of frequency-locked oscillators. As K is further increased, the size of the locked population grows, and a second transition may occur beyond which all of oscillators are locked at the same frequency. While the former transition is better studied, for our purposes the latter transition is more important.

As a nonlinear dynamical system with little or no symmetry, equation (3) has complicated solutions. However, in the large-N limit and treated statistically, the model is surprisingly tractable: the above-mentioned transitions can be calculated using a self-consistency approach [10, 11]. The essential points are as follows. The first step is to define the complex order parameter

$$\sigma e^{\imath\psi} = \frac{1}{N}\sum_{\ell=1}^{N} e^{\imath\theta_\ell} \tag{4}$$

where σ and ψ are real. The amplitude $\sigma \in [0, 1]$ is a measure of the overall phase coherence of the system. Typical numerical simulations of large populations find that the order parameter settles down to a uniformly rotating state $\sigma e^{\imath\Omega t}$ where σ and Ω are approximately constant. Next, use equation (4) to rewrite equation (3) as

$$\dot{\theta}_j = \omega_j - K\sigma\sin\left(\theta_j - \psi + \alpha\right). \tag{5}$$

Transform to a rotating frame such that $\varphi_j = \theta_j - \Omega t + \alpha$, so that

$$\dot{\varphi}_j = \omega_j - \Omega - K\sigma\sin\varphi_j. \tag{6}$$

One sees immediately that, treating σ and Ω as constants, the population of oscillators partitions into two groups, those that reach a fixed phase (in the rotating frame), and those whose phases drift monotonically around the circle. The former group represents the frequency-locked sub-population, comprising oscillators having bare frequencies satisfying $|\omega_j - \Omega| \leqslant K\sigma$; these evolve to a constant phase such that $\sin\varphi_j = \frac{\omega_j - \Omega}{K\sigma}$. Meanwhile, each oscillator outside the locking interval winds at a dressed frequency $\tilde{\omega}_j$ (in the rotating frame) which is determined by direct integration of equation (6),

$$\tilde{\omega}_j^2 = \left(\omega_j - \Omega\right)^2 - \left(K\sigma\right)^2. \tag{7}$$

Now, whether or not the oscillator falls inside the locking interval, equation (6) is readily solved. The basic idea is to substitute the solutions back into equation (4), thus generating a self-consistency condition for the parameters σ and Ω. In the limit $N \to \infty$,

$$\sigma e^{\imath\alpha} = \int\int d\omega\, d\varphi\, g(\omega)\, \rho(\varphi|\omega)\, e^{\imath\varphi} \tag{8}$$

where $\rho(\varphi|\omega)$ is the conditional (stationary) density of phases for oscillators with bare frequency ω. For oscillators in the locked interval, so that $-K\sigma < \omega - \Omega < K\sigma$, the conditional density is concentrated

$$\rho(\varphi|\omega) = \delta\left(\varphi - \arcsin\left[\frac{\omega-\Omega}{K\sigma}\right]\right) \tag{9}$$

where δ is the Dirac delta function. For oscillators outside the locked interval the conditional density is distributed around the circle:

$$\rho(\varphi|\omega) = \frac{\sqrt{(\omega-\Omega)^2 - (K\sigma)^2}}{2\pi\,|\omega - \Omega - \sin\varphi|}. \tag{10}$$

Substitution of equations (9) and (10) into equation (8) leads to, after some additional effort, the following useful form of the self-consistency condition [10]:

$$\sigma e^{\imath\alpha} = K\sigma\left(\imath J + \int_{-\pi/2}^{\pi/2} d\xi\, g\left(\Omega + K\sigma\sin\xi\right)\, e^{\imath\xi}\cos\xi\right) \tag{11}$$

where

$$J = \int_0^{\pi/2} d\xi \frac{\cos\xi\,(1-\cos\xi)}{\sin^3\xi}\left[g\left(\Omega+\mu\right) - g\left(\Omega-\mu\right)\right] \tag{12}$$

and $\mu = K\sigma/\sin\xi$. Starting from the given parameters K, α, and function $g(\omega)$, one solves equation (11)—typically numerically—to find σ and Ω; these are used in turn to determine the fraction of frequency-locked oscillators:

$$f = \int_{\Omega-K\sigma}^{\Omega+K\sigma} d\omega\, g\left(\omega\right). \tag{13}$$

Full frequency-locking corresponds to $f = 1$.

The goal, then, is to map the dynamical equations for a Josephson array onto the Kuramoto–Sakaguchi equation, and in so doing determine K, α, and $g(\omega)$ in terms of the circuit parameters, including the distribution-widths of the junction parameters. From there, the degree of frequency-locking is readily determined.

3. Series array of point contact junctions

A circuit schematic is shown in figure 1. The governing dynamical equations are

$$\frac{\hbar}{2er_j}\dot{\phi}_j + I_j\sin\phi_j = B - \dot{Q} \quad ; \quad j = 1, 2, \ldots, N \tag{14}$$

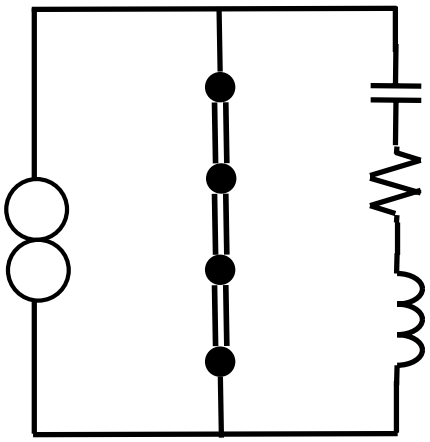

Figure 1. Circuit schematic of a series array. The filled circles represent superconducting islands, the double-lines represent Josephson junctions. The array is driven by a constant current source (double circle) and coupled to an external load (inductor-resistor-capacitor combination).

$$L\ddot{Q} + R\dot{Q} + \frac{Q}{C} = \sum_{\ell=1}^{N} \frac{\hbar}{2e}\dot{\phi}_\ell \tag{15}$$

where r_j is the jth junction's normal resistance and I_j is its critical current, B is the externally-supplied bias current, Q is the charge on the load capacitor, L, R, and C are the load inductance, resistance, and capacitance. In what follows, the disorder and coupling are assumed to be weak. In this regime, equations (14) and (15) can be mapped onto equation (3) using a so-called averaging method [12], as now described.

Assume the bias current B is large enough that $\dot{\phi}_j$ is always positive. The first step is to introduce the 'natural angle' variables defined by

$$\frac{2er_j}{\hbar}\frac{\mathrm{d}\theta_j}{\omega_j} = \frac{\mathrm{d}\phi_j}{B - I_j \sin\phi_j} \tag{16}$$

where ω_j is the frequency of an isolated junction

$$\omega_j = \frac{2er_j}{\hbar}\left(B^2 - I_j^2\right)^{1/2}. \tag{17}$$

The θ_j are natural in the sense that, in the uncoupled limit, they advance uniformly, while the ϕ_j do not. Direct integration of equation (16) yields

$$B - I_j \sin\phi_j = \frac{B^2 - I_j^2}{B - I_j \cos\theta_j} \tag{18}$$

so that equation (14) can be rewritten as

$$\dot{\theta}_j = \omega_j - \frac{\omega_j \dot{Q}}{B^2 - I_j^2}\left(B - I_j \cos\theta_j\right). \tag{19}$$

For weak disorder, it is convenient to write

$$r_j = \bar{r}\,(1 + \varepsilon\rho_j) \tag{20a}$$

$$I_{cj} = \bar{I}\,(1 + \varepsilon\zeta_j) \tag{20b}$$

$$\omega_j = \bar{\omega}\,(1 + \varepsilon\delta_j) \tag{20c}$$

where ε is a formal parameter used to keep track of small quantities; it will be set to one at the end. The overbar denotes a sample mean. Note that ρ_j, ζ_j, and δ_j are not independent: to leading order,

$$\delta_j = \rho_j - \frac{\bar{I}}{B^2 - \bar{I}^2}\zeta_j + O(\varepsilon). \tag{21}$$

In what follows, assume that the bias current is not too close to the (largest) critical current and that the coupling weak, so that $B - I_j > O(\varepsilon)$, and $\dot{Q} = O(\varepsilon)$, respectively. Equation (19) becomes

$$\dot{\theta}_j = \bar{\omega} + \varepsilon\bar{\omega}\delta_j - \frac{\bar{\omega}\dot{Q}}{B^2 - \bar{I}^2}\left(B - \bar{I}\cos\theta_j\right) + O(\varepsilon^2). \tag{22}$$

The basic idea behind the averaging method is as follows. To leading order, $\theta_j(t) = \theta_j(0) + \bar{\omega}t$, so substituting this into the already-small term in equation (22), generates an error of $O(\varepsilon^2)$. Moreover, since $\theta_j - \bar{\omega}t$ is slowly varying, we can replace the righthand side by its time average over one cycle, again at the cost of an $O(\varepsilon^2)$ error. To carry out the latter step, we need an explicit expression for $\dot{Q}$. From equations (14) and (18),

$$\frac{\hbar}{2e}\dot{\phi}_j = \frac{B^2 - I_j^2}{B - I_j\cos\theta_j}r_j - \dot{Q}r_j \tag{23}$$

so that equation (15) becomes, to leading order in ε

$$L\ddot{Q} + (R + N\bar{r}) + \frac{1}{C}Q = \bar{r}\left(B^2 - \bar{I}^2\right)\sum_{\ell=1}^{N}\sum_{n=0}^{\infty}A_n\cos\left[n\bar{\omega}t + n\theta_\ell(0)\right] \tag{24}$$

where I have introduced the Fourier series

$$\sum_{n=0}^{\infty}A_n\cos n\bar{\omega}t = \left[B - \bar{I}\cos\bar{\omega}t\right]^{-1}. \tag{25}$$

Equation (24) is the standard equation for a periodically driven linear oscillator. It is evident from equation (22) that only the fundamental-frequency component of Q will survive the time averaging. This component is, in steady state,

$$Q(t) = \sum_{k=1}^{N}\mathcal{B}_1\cos\left[\bar{\omega}t + \theta_k(0) + \beta_1\right] \tag{26}$$

where

$$\mathcal{B}_1^2 = \frac{\bar{r}^2\left(B^2 - \bar{I}^2\right)^2 A_1^2}{\left(L\bar{\omega}^2 - 1/C\right)^2 + \bar{\omega}^2\left(R + N\bar{r}\right)^2} \tag{27}$$

and

$$\beta_1 = \arctan\left\{\frac{\overline{\omega}\,(R+N\overline{r})}{L\overline{\omega}^2 - 1/C}\right\}. \tag{28}$$

Substitution of equation (26) into equation (22) and taking the time average over one period yields

$$\dot{\theta}_j = \overline{\omega} + \varepsilon\overline{\omega}\delta_j - \frac{\overline{\omega}^2\overline{I}}{B^2 - \overline{I}^2}\frac{\mathcal{B}_1}{2}\sum_{k=1}^{N}\sin\left(\theta_k - \theta_j + \beta_1\right). \tag{29}$$

Finally, set $\alpha = \beta_1 + \pi$, so that

$$\dot{\theta}_j = \omega_j + \frac{K}{N}\sum_{k=1}^{N}\sin\left(\theta_k - \theta_j + \alpha\right) \tag{30}$$

where

$$K = \frac{N\overline{r}\overline{\omega}\left(\frac{2e}{\hbar}\overline{r}B - \overline{\omega}\right)}{\left[\left(L\overline{\omega}^2 - 1/C\right)^2 + \overline{\omega}^2\left(R + N\overline{r}\right)^2\right]^{1/2}} \tag{31}$$

and

$$\cos\alpha = \frac{L\overline{\omega}^2 - 1/C}{\left[\left(L\overline{\omega}^2 - 1/C\right)^2 + \overline{\omega}^2\left(R + N\overline{r}\right)^2\right]^{1/2}} \tag{32}$$

with $0 \leqslant \alpha \leqslant \pi/2$. This completes the task of mapping the governing dynamical equations (14) and (15) onto the Kuramoto–Sakaguchi model equation (3).

Two remarks are in order. First, in the circuit problem, the natural control parameter is the bias current, but the effective coupling parameters K and α are not monotonic functions B. Similarly, the effective disorder also varies with the control parameter B. Since it is the interplay between coupling and disorder that determines the degree of synchronization, it's difficult to extract a simple heuristic condition for achieving full-locking. Second, the derived values of the coupling parameters K and α are independent of the disorder, while the bare frequencies $\{\omega_j\}$ are determined by the single junction problem, independent of the coupling. In subsequent sections, we will take advantage of this decomposition to streamline the calculations.

4. Series array of tunnel junctions

For a series array of tunnel junctions, the governing dynamical equations are

$$\frac{\hbar c_j}{2e}\ddot{\phi}_j + \frac{\hbar}{2er_j}\dot{\phi}_j + I_j\sin\phi_j = B - \dot{Q} \quad ; \quad j = 1, 2, \ldots, N \tag{33}$$

$$L\ddot{Q} + R\dot{Q} + \frac{Q}{C} = \sum_{\ell=1}^{N}\frac{\hbar}{2e}\dot{\phi}_\ell \tag{34}$$

where c_j is the capacitance of the jth tunnel junction, and all other quantities are as previously defined. The new stumbling block is that we do not know the transformation to natural

angles that would allow a repeat of the averaging calculation. Instead, we will use an expansion technique, originally applied to the identical-element Josephson array by Chernikov and Schmidt [13].

4.1. Bare frequencies

We first determine the bare frequencies, i.e. an expression analogous to equation (17). Consider a single isolated junction

$$\frac{\hbar c}{2e}\ddot{\phi}+\frac{\hbar}{2er}\dot{\phi}+I\sin\phi=B. \tag{35}$$

Ranging over parameter space, equation (35) admits fixed point and periodic attractors—including regions of bistability—and homclinic orbits, as described in [14]. In this paper, we confine attention to the periodic state.

Introduce the dimensionless time $\tau=\nu t$, so that

$$\beta\phi''+\phi'+\gamma\sin\phi=1 \tag{36}$$

where the prime denotes differentiation with respect to τ, and

$$\nu=(2erB)/\hbar \tag{37}$$

$$\beta=\hbar c\nu^2/(2eB) \tag{38}$$

$$\gamma=I/B. \tag{39}$$

The idea is to develop a solution for $\phi(\tau)$ using γ as an expansion parameter. We will carry this through second order. Substitute

$$\phi=\phi_0+\gamma\phi_1+\gamma^2\phi_2+\ldots \tag{40}$$

into equation (36), and equate terms of equal order in γ. At zeroth order,

$$\beta\phi_0''+\phi_0'=1 \qquad \Rightarrow \qquad \phi_0=\theta+\tau \tag{41}$$

where θ is a constant. At first order in γ,

$$\beta\phi_1''+\phi_1'+\sin\phi_0=0 \qquad \Rightarrow \qquad \phi_1=A\sin\tau+B\cos\tau \tag{42}$$

where A and B are constants. Using the expression for ϕ_0, one readily finds

$$\begin{pmatrix}A\\B\end{pmatrix}=\left(1+\beta^2\right)^{-1}\begin{pmatrix}\beta & -1\\ 1 & \beta\end{pmatrix}\begin{pmatrix}\cos\theta\\ \sin\theta\end{pmatrix}. \tag{43}$$

At second order in γ,

$$\beta\phi_2''+\phi_2'+\phi_1\cos\phi_0=0 \qquad \Rightarrow \qquad \phi_2=\lambda\tau+E\sin 2\tau+F\cos 2\tau \tag{44}$$

where λ, E, and F are constants. Using the expressions for ϕ_0 and ϕ_1, one finds

$$\lambda=-\frac{1}{2}\left(1+\beta^2\right)^{-1}. \tag{45}$$

Through order γ^2, then,

$$\phi(\tau)=\theta+\tau+\gamma(A\sin\tau+B\cos\tau)+\gamma^2(\lambda\tau+E\sin 2\tau+F\cos 2\tau). \tag{46}$$

The period T satisfies

$$\phi(T) - \phi(0) = 2\pi. \tag{47}$$

Introduce the expansion $T = T_0 + \gamma T_1 + \gamma T_2 + \ldots$ into equation (46) evaluated at $\tau = T$, and solve order-by-order in γ, to find

$$T = 2\pi\left(1 - \gamma^2\lambda\right) + O(\gamma^3). \tag{48}$$

In terms of the original units the frequency is $2\pi\nu/T$. For a tunnel junction with parameters r_j, c_j, and I_j, this gives the bare frequency

$$\omega_j = \frac{2er_jB}{\hbar}\left(1 - \frac{1}{2}\left(1+\beta_j^2\right)^{-1}\left(\frac{I_j}{B}\right)^2\right) \tag{49}$$

where $\beta_j = 2er_j^2c_jB/\hbar$. To this same level of accuracy, equation (49) can be written in a form that invites direct comparison with the point contact formula equation (17):

$$\omega_j = \frac{2er_j}{\hbar}\sqrt{B^2 - z_jI_j^2} \tag{50}$$

where $z_j = \left(1+\beta_j^2\right)^{-1}$.

4.2. Effective coupling parameters

To calculate K and α, it's sufficient to consider the identical-junction problem. Using the dimensionless time $\tau = \nu t$, and dimensionless charge $q = \nu Q/I_b$, equations (33) and (34) become

$$\beta\phi_j'' + \phi_j' + \gamma\sin\phi_j = 1 - q' \tag{51}$$

$$q'' + \Gamma q' + \Omega^2 q = \mu\sum_{\ell=1}^{N}\phi_\ell' \tag{52}$$

where ν, β, and γ are defined by equations (37)–(39); and

$$\Gamma = \frac{R}{L\nu} \tag{53}$$

$$\Omega^2 = \left(CL\nu^2\right)^{-1} \tag{54}$$

$$\mu = \frac{\hbar}{2eBL}. \tag{55}$$

As before, develop a solution in powers of γ:

$$\phi_j = \phi_j^{(0)} + \gamma\phi_j^{(1)} + \gamma^2\phi_j^{(2)} + \ldots \tag{56}$$

$$q = q^{(0)} + \gamma q^{(1)} + \gamma^2 q^{(2)} + \ldots \tag{57}$$

and solve order by order. The algebra is considerably more tedious than for the isolated junction, and the details are relegated to the appendix. Through second order, the steady state solution has the form

$$\phi_j(\tau) = \theta_j + \tau + \gamma\left(A_j \sin\tau + B_j \cos\tau\right) + \gamma^2\left(\lambda_j \tau + E_j \sin 2\tau + F_j \cos 2\tau\right) \tag{58}$$

$$q(\tau) = q_0 + \gamma\left(C \sin\tau + D\cos\tau\right) + \gamma^2\left(G\sin 2\tau + H\cos 2\tau\right) \tag{59}$$

where the constants $A_j, B_j, \lambda_j, E_j, F_j, C, D, G$, and H can be expressed in terms of the 'initial conditions' $(q_0, \{\theta_j\})$. Equation (58) can be used to generate a discrete map of the phase dynamics. Starting at $\tau = 0$, advancing $\tau \to 2\pi$ results in advancing $\phi_j \to \phi_j + 2\pi\left(1 + \gamma^2\lambda_j\right)$. This is equivalent to keeping $\tau = 0$ while advancing $\theta_j \to \theta_j + 2\pi\left(1 + \gamma^2\lambda_j\right)$. In other words, propagating ϕ_j over a time interval $\Delta\tau = 2\pi$ is equivalent to the map iteration

$$\theta_j \to \theta_j + 2\pi\left[1 + \gamma^2\lambda_j\left(\vec{\theta}\right)\right]$$

where the notation emphasizes that each λ_j is a function of $\theta_1, \theta_2, \ldots$. The θ_j advance at a nearly uniform rate, so the map is well-approximated by the differential equations

$$\frac{\Delta\theta_j}{\Delta\tau} \approx \theta_j' = 1 + \gamma^2\lambda_j.$$

Upon explicit evaluation of the coefficients, one finds (see appendix)

$$\lambda_j = \frac{-1}{2\left(1+\beta^2\right)} - \frac{m_1}{2}\sum_\ell \sin\left(\theta_\ell - \theta_j\right) + \frac{m_2}{2}\sum_\ell \cos\left(\theta_\ell - \theta_j\right) \tag{60}$$

where m_1 and m_2 are (somewhat complicated) functions of the load and junction parameters. In terms of the unscaled time, $\dot{\theta}_j = \nu\theta_j'$, so we recover the zero-disorder limit of the Sakaguchi–Kuramoto model

$$\dot{\theta}_j = \omega + \frac{K}{N}\sum_\ell \sin\left(\theta_\ell - \theta_j + \alpha\right) \tag{61}$$

where

$$\omega = \nu\left[1 - \frac{1}{2}\gamma^2\left(1+\beta^2\right)\right] \tag{62}$$

$$K = \frac{1}{2}N\gamma^2\nu\sqrt{m_1^2 + m_2^2} \tag{63}$$

$$\alpha = \arctan\left(-m_2/m_1\right). \tag{64}$$

The result for ω recovers the previously derived equation (49), as expected. The expressions for K and α are the main results of this subsection. The full problem, with disorder, is given by equation (61) with ω replaced by ω_j from equation (50), and (K, α) evaluated from equations (63) and (64) using the mean junction parameter values.

5. Two dimensional array of point contact junctions

The architecture in a standard rectangular array consists of an N rows and M columns of superconducting islands, with bias current injected along the top, and removed along the bottom (see figure 2). Denote the superconducting phase of the island in row n and column m by Ψ_{nm}.

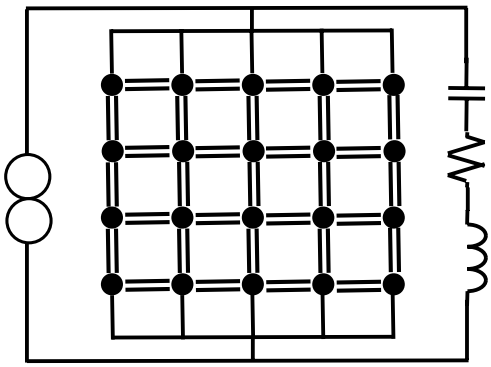

Figure 2. Schematic of a two-dimensional array, current biased, with an external load.

The overall phase shift invariance reduces the number of island phase variables to $NM-1$. The equations of motion can be written

$$\sum_{\langle k\ell\rangle}\left[\frac{\hbar}{2er_{ij,k\ell}}\left(\dot{\Psi}_{ij}-\dot{\Psi}_{k\ell}\right)+I^{c}_{ij,k\ell}\sin\left(\Psi_{ij}-\Psi_{k\ell}\right)\right]=I_{ij} \tag{65}$$

$$\mathcal{L}\ddot{Q}+\mathcal{R}\dot{Q}+\frac{Q}{\mathcal{C}}=\frac{\hbar}{2e}\sum_{i=1}^{N-1}\left(\dot{\Psi}_{i+1j}-\dot{\Psi}_{ij}\right) \tag{66}$$

where equation (65) hold for each site (i,j) and the sum is over all nearest-neighbor islands; equation (66) holds for each column j; I_{ij} is the externally-supplied current into island (i,j); and $r_{ij,k\ell}$ and $I^{c}_{ij,k\ell}$ are the resistance and critical current, respectively, of the junction linking island (i,j) and (k,ℓ). The notation for the load parameters $\mathcal{L},\mathcal{R},\mathcal{C}$ is made in anticipation of later comparison with the corresponding series array.

Equivalently, the dynamics can be described in terms of the more numerous Josephson junction phase differences, supplemented by constraint equations. Specifically, there are $N(M-1)$ horizontal junctions, $(N-1)M$ vertical junctions, for a total of $2NM-N-M$ Josephson phase variables, and one constraint equation for each of the $(N-1)(M-1)$ plaquettes, so that there are $NM-1$ free variables, as before. The labeling scheme is shown in figure 3. Let H_{nm} be the Josephson phase of a horizontal junction, V_{nm} the Josephson phase of a vertical junction, and Δ_{nm} the mesh current of a plaquette. The equations of motion are

$$\frac{\hbar}{2e\tilde{r}_{mn}}\dot{H}_{\mathrm{nm}}+\tilde{I}_{\mathrm{nm}}\sin H_{\mathrm{nm}}=\Delta_{\mathrm{nm}}-\Delta_{n-1m} \tag{67}$$

$$\frac{\hbar}{2er_{\mathrm{nm}}}\dot{V}_{\mathrm{nm}}+I_{\mathrm{nm}}\sin V_{\mathrm{nm}}=B_{m}+\Delta_{nm-1}-\Delta_{\mathrm{nm}} \tag{68}$$

$$L_{\mathrm{nm}}\Delta_{\mathrm{nm}}=-\frac{\hbar}{2e}\left(H_{\mathrm{nm}}+V_{nm+1}-H_{n+1m}-V_{\mathrm{nm}}\right) \tag{69}$$

$$\mathcal{L}\ddot{Q}+\mathcal{R}\dot{Q}+\frac{Q}{\mathcal{C}}=\frac{\hbar}{2e}\sum_{n=1}^{N}\dot{V}_{\mathrm{nm}} \tag{70}$$

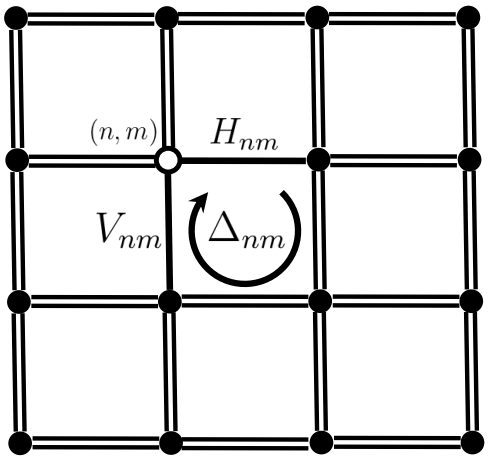

Figure 3. Portion of a 2D array illustrating the labeling scheme. The open circle denotes the superconducting island at position (n,m); the single-line bonds identify the labeled horizontal and vertical junctions; $\Delta_{\rm nm}$ is a mesh current.

where, $\tilde{r}_{\rm nm}$ is the resistance of the corresponding horizontal junction and $\tilde{I}_{\rm nm}$ is its critical current, $r_{\rm nm}$ is the resistance of the corresponding vertical junction and $I_{\rm nm}$ is its critical current. Finally, B_m is the portion of the bias current feeding the mth vertical column, so that the total bias current is $MB = \sum_\ell B_\ell + \dot{Q}$.

In either form equations (65) and (66) or equations (67)–(70), the governing dynamical equations are significantly more complicated than those of the series array equations (14) and (15). Nevertheless, the anisotropy of the bias current induces an anisotropic response which radically simplifies the analysis: the horizontal junctions pass only small currents, and the array quickly settles into a steady state such that the vertical junctions within each row are frequency-locked and nearly in-phase. At the same time, despite the strong frequency-locking within each row, the various rows hardly influence each other at all. This behavior was noted in early numerical studies of rectangular arrays, with [16] and without [17] external loads.

5.1. Intra-row locking and effective frequencies

We first consider the strong interactions within a given row. Specifically, we ask: if the junctions are not identical, but the vertical junctions lock to a common frequency, what will that frequency be? Consider a single, isolated row as shown in figure 4. The current $\hat{I}_j$ passing through the jth vertical junction is (suppressing the row index)

$$\hat{I}_j = B + \Delta_{j-1} - \Delta_j \quad ; \quad j = 1, 2, \ldots, M \tag{71}$$

where Δ_j is the mesh current in the jth plaquette and by definition $\Delta_0 = 0 = \Delta_M$. Now, if $\hat{I}_j$ were constant, then the exact expression for the frequency of the jth vertical junction would be, assuming $\hat{I}_j > I_j^2$,

$$\omega_j = \frac{2er_j}{\hbar}\left(\hat{I}_j^2 - I_j^2\right)^{1/2}. \tag{72}$$

If all of the vertical junctions within the row are to lock at the same frequency ω, then just the right amount of current must be shunted across the horizontal junctions to compensate

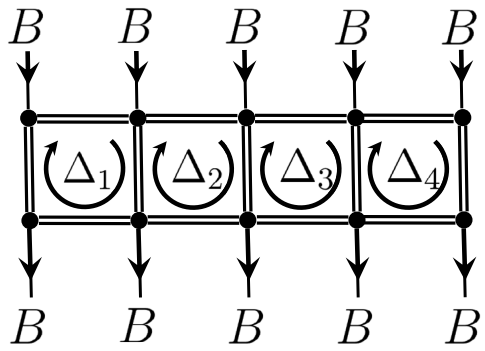

Figure 4. Horizontal slice of the two dimensional array.

for the variations in their resistances and critical currents. Combining equations (71) and (72) yields, to first order in Δ_j,

$$\left(\frac{\hbar\omega}{2er_j}\right)^2 = B^2 - I_j^2 + 2B\left(\Delta_{j-1} - \Delta_j\right). \tag{73}$$

Summing over all j, the mesh currents drop out, with result

$$\omega^2 = \left(\frac{2e}{\hbar}\right)^2 \frac{B^2 - \langle I^2\rangle}{\langle r^{-2}\rangle} \tag{74}$$

where I have introduced the row-averaged quantities

$$\langle r^{-2}\rangle = \frac{1}{M}\sum_{\ell=1}^{M} r_\ell^{-2} \tag{75}$$

$$\langle I^2\rangle = \frac{1}{M}\sum_{\ell=1}^{M} I_\ell^2. \tag{76}$$

Equation (74) gives the common frequency of all the vertical junctions in the row, in terms of the set of individual junction parameters r_j, I_j. Therefore, the probability density of the row-frequencies is

$$\rho_\omega(\omega) = \iint \rho_J(r,I)\delta\left(\omega - \omega(r,I)\right)\mathrm{d}r\,\mathrm{d}I$$

where $\rho_J(r,I)$ is the joint probability density of a junction's resistance and critical current. One sees that the row-averaging reduces the effective disorder [16–18]: since $\langle r^{-2}\rangle$ and $\langle I^2\rangle$ are each the average of M independent random variables, their variances are smaller by a factor M compared with the single-element values.

5.2. Effective coupling constants

The next step is to show that the disorder-free system reduces to a corresponding disorder-free Kuramoto–Sakaguchi system, and in so doing to determine the coupling parameters. To this end, in equations (67)–(70), set all resistances to $\bar{r}$, critical currents to $\overline{I_c}$, and plaquette

inductances to $\overline{L}$. Assuming in-phase synchronization within each row, set $H_{\rm nm} = 0$ and $\Delta_{\rm nm} = 0$, automatically satisfying equations (67) and (69), and leaving

$$\frac{\hbar}{2e\overline{r}}\dot{V}_{\rm nm} + \overline{I}_c \sin V_{\rm nm} = B_m \tag{77}$$

$$\mathcal{L}\ddot{Q} + \mathcal{R}\dot{Q} + \frac{Q}{\mathcal{C}} = \frac{\hbar}{2e}\sum_{n=1}^{N}\dot{V}_{\rm nm}. \tag{78}$$

Meanwhile, a portion $\dot{Q}$ of the total bias current MB runs through the load, and the remainder, by symmetry, splits equally along each column, so $B_m = B - \dot{Q}/M$:

$$\frac{\hbar}{2e\overline{r}}\dot{V}_{\rm nm} + \overline{I}_c \sin V_{\rm nm} = B - \frac{\dot{Q}}{M}. \tag{79}$$

Comparison of equations (78) and (79) with the zero disorder limit of the series array equations (14) and (15) show that these are identical, provided the load is scaled according to $\mathcal{L} = L/M$, $\mathcal{R} = R/M$, $\mathcal{C} = MC$. (This scaling is precisely what one would expect intuitively for a matched load: the equivalent resistance of an array with M parallel columns is smaller by a factor of M, with corresponding statements for the inductance and capacitance.) We can immediately carry over the results for K and α, given by equations (31) and (32).

6. Two dimensional arrays of tunnel junctions

The calculations closely parallel those of the previous section. The circuit equations are

$$\frac{\hbar\tilde{c}_{\rm nm}}{2e}\ddot{H}_{\rm nm} + \frac{\hbar}{2e\tilde{r}_{\rm nm}}\dot{H}_{\rm nm} + \tilde{I}_{\rm nm}\sin H_{\rm nm} = \Delta_{\rm nm} - \Delta_{n-1m} \tag{80}$$

$$\frac{\hbar c_{\rm nm}}{2e}\ddot{V}_{\rm nm} + \frac{\hbar}{2er_{\rm nm}}\dot{V}_{\rm nm} + I_{\rm nm}\sin V_{\rm nm} = \Delta_{nm-1} - \Delta_{\rm nm} \tag{81}$$

$$L_{\rm nm}\Delta_{\rm nm} = -\left(H_{\rm nm} + V_{nm+1} - H_{n+1m} - V_{\rm nm}\right) \tag{82}$$

$$\mathcal{L}\ddot{Q} + \mathcal{R}\dot{Q} + \frac{Q}{\mathcal{C}} = \frac{\hbar}{2e}\sum_{n=1}^{N-1}\dot{V}_{\rm nm} \tag{83}$$

where the new parameters are $\tilde{c}_{\rm nm}$ for the horizontal junctions and $c_{\rm nm}$ for the vertical junctions.

6.1. Intra-row locking and effective frequencies

Consider a single row of junctions as in figure 4. The current through the jth vertical junction is (suppressing the row index)

$$\hat{I}_j = B + \Delta_{j-1} - \Delta_j \quad ; \quad j = 1, 2, \ldots, M. \tag{84}$$

If $\hat{I}_j$ were constant, the oscillation frequency of the jth vertical junction would be (approximately) given by equation (50)

$$\omega_j = \frac{2er_j}{\hbar}\sqrt{\hat{I}_j^2 - z_j I_j^2} \tag{85}$$

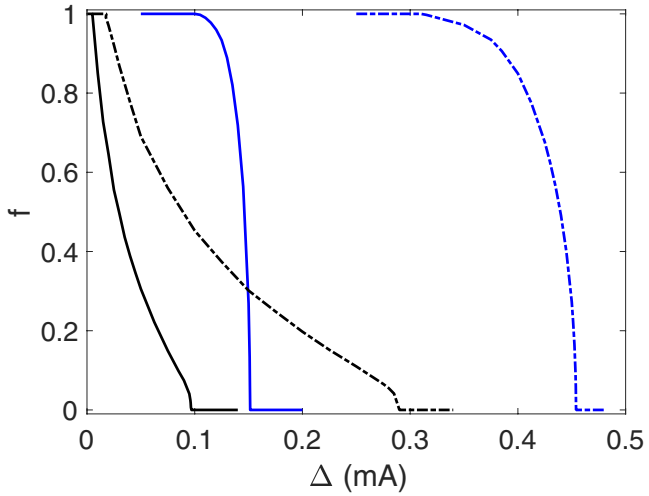

Figure 5. Fraction of frequency-locked junctions versus critical-current disorder Δ. Curves are for: series array of point contact junctions (solid black), series array of tunnel junctions (solid blue), rectangular array of point contact junctions (dot-dash black), and rectangular array of tunnel junctions (dot-dash blue). Parameter values: $\bar{r} = 0.4$ ohms, $\bar{I} = 0.5$ mA, $\bar{\beta} = 1.0$; for series arrays $N = 100$, $B = 1.5$ mA, $R = 50$ ohms, $L = 25$ pH, and $C = 0.04$ pF; for rectangular arrays $N = 100$, $M = 9$, $\mathcal{R} = R/M$, $\mathcal{L} = L/M$, $\mathcal{C} = MC$, and bias current MB.

where $z_j = \left(1 + \beta_j^2\right)^{-1}$. For small disorder, and thus small mesh currents, combine the last two equations to get

$$\left(\frac{\hbar\omega}{2er_j}\right)^2 = B^2 - z_j I_j^2 + 2B\left(\Delta_{j-1} - \Delta_j\right) \tag{86}$$

to first order in Δ_j. Summing over all j, the mesh currents drop out, and so

$$\omega^2 = \left(\frac{2e}{\hbar}\right)^2 \frac{B^2 - \langle zI^2\rangle}{\langle r^{-2}\rangle} \tag{87}$$

where $\langle r^{-2}\rangle$ is given by equation (75) and

$$\langle zI^2\rangle = \frac{1}{M}\sum_{\ell=1}^{M} z_\ell I_\ell^2. \tag{88}$$

6.2. Effective coupling constants

The equations of motion for the disorder-free system admit row-synchronized solutions $H_{\rm nm} = 0$, $\Delta_{\rm nm} = 0$, so that (compare equations (78) and (79))

$$\frac{\hbar\bar{c}}{2e}\ddot{V}_{\rm nm} + \frac{\hbar}{2e\bar{r}}\dot{V}_{\rm nm} + \bar{I}_c \sin V_{\rm nm} = B - \frac{\dot{Q}}{M} \tag{89}$$

$$\mathcal{L}\ddot{Q} + \mathcal{R}\dot{Q} + \frac{Q}{\mathcal{C}} = \frac{\hbar}{2e}\sum_{\ell=1}^{N-1}\dot{V}_\ell. \tag{90}$$

For the properly scaled load parameters $\mathcal{L} = L/M$, $\mathcal{R} = R/M$, $\mathcal{C} = MC$, these are equivalent to the governing equations for a series array of identical tunnel junctions, equations (33) and (34), so the effective coupling constants are given by equations (63) and (64).

7. Discussion

In each of four cases, we mapped the Josephson junction array dynamics onto the Kuramoto–Sakaguchi model. The reduced model is fully tractable: a self-consistency method determines quantitatively the effect of disorder on the degree of mutual frequency-lock.

What practical advantage does this reduction afford over direct numerical simulations? The latter uses as input the distributions of junction parameters $\{r_i,\}, \{I_i\}$, and $\{\beta_i\}$; the load parameters B, R, L, and C; and the array parameters N, M, and $\{L_{\rm nm}\}$; in addition, ensemble averaging requires multiple runs over the sampled disorder. Meanwhile, the reduced model needs only the distribution of bare frequencies $\{\omega_j\}$, the coupling constants K and α, and the array dimensions N, M; and its algebraic solution automatically embodies ensemble averaging.

Aside from improved efficiency, mapping the various cases onto the same reduced model allows direct comparison and a quantitative assessment of their relative merits. As stated in the introduction, a key consideration for applications is the degree to which disorder can be overcome to achieve complete frequency locking. Qualitatively, one expects tunnel junctions to provide some advantage over point contact junctions because the junction capacitance introduces an additional tuning parameter. Similarly, rectangular arrays should show better disorder-tolerance than their series-array counterparts thanks to spontaneous intra-row frequency-locking [15, 19].

To make these observations concrete and quantitative, we apply the results of this paper to a particular example using a normalized parabolic distribution $P(I)$ for the critical currents with mean $\bar{I}$ and full width 2Δ:

$$P(I) = \frac{3}{4\Delta}\left[\Delta^2 - \left(I - \bar{I}\right)^2\right]. \tag{91}$$

For simplicity, the junction resistances and capacitances are taken to be identical. The series arrays contain $N = 100$ junctions each; the rectangular arrays consist of $N = 100 \times M = 900$ superconducting islands, and the load parameters are appropriately scaled with M. The choice of $\overline{\beta} = 1$ was made because it seems to give the best performance. Figure 5 shows the fraction of frequency-locking f versus disorder. The data clearly shows the expected improvement of $\sim \sqrt{M}$ for the rectangular arrays. Also conspicuous is the relative steepness of the tunnel junction curves, as compared with the point contact junctions, though a simple physical explanation for this is unknown.

Appendix. Tunnel junction series array

The goal is to calculate the effective coupling constants K an α starting from equations (51) and (52), using the expansions equations (56) and (57). At zeroth order in γ,

$$\begin{aligned} \beta\phi_j^{0\prime\prime} + \phi_j^{0\prime} &= 1 - q_0' \\ q_0'' + \Gamma q_0' + \Omega^2 q_0 &= \mu \sum_\ell \phi_\ell^{0\prime} \end{aligned} \tag{A.1}$$

which has steady state solution

$$\begin{aligned}\phi_j^0 &= \theta_j + \tau \\ q_0 &= \mu N \Omega^{-2}.\end{aligned} \tag{A.2}$$

At first order in γ,

$$\begin{aligned}\beta\phi_j^{1\prime\prime} + \phi_j^{1\prime} + \sin\phi_j^0 &= -q_1' \\ q_1'' + \Gamma q_1' + \Omega^2 q_1 &= \mu\sum_\ell \phi_\ell^{1\prime}\end{aligned} \tag{A.3}$$

which has steady state solution of the form

$$\begin{aligned}\phi_j^1 &= A_j\sin\tau + B_j\cos\tau \\ q_1 &= C\sin\tau + D\cos\tau.\end{aligned} \tag{A.4}$$

Substitute equation (A.4) into equation (A.3), and separately balance the $\sin\tau$ and $\cos\tau$ terms, to get

$$\begin{pmatrix}-\beta & -1\\ 1 & -\beta\end{pmatrix}\begin{pmatrix}A_j\\ B_j\end{pmatrix} = \begin{pmatrix}0 & 1\\ -1 & 0\end{pmatrix}\begin{pmatrix}C\\ D\end{pmatrix} - \begin{pmatrix}\cos\theta_j\\ \sin\theta_j\end{pmatrix} \tag{A.5}$$

and

$$\begin{pmatrix}\Omega^2-1 & -\Gamma\\ \Gamma & \Omega^2-1\end{pmatrix}\begin{pmatrix}C\\ D\end{pmatrix} = \mu\begin{pmatrix}0 & -1\\ 1 & 0\end{pmatrix}\begin{pmatrix}\sum_\ell A_\ell\\ \sum_\ell B_\ell\end{pmatrix}. \tag{A.6}$$

At second order in γ,

$$\begin{aligned}\beta\phi_j^{2\prime\prime} + \phi_j^{2\prime} + \phi_j^1\cos\phi_j^0 &= -q_2' \\ q_2'' + \Gamma q_2' + \Omega^2 q_2 &= \mu\sum_\ell \phi_\ell^{2\prime}\end{aligned} \tag{A.7}$$

where

$$2\phi_j^1\cos\phi_j^0 = A_j\sin\theta_j - B_j\cos\theta_j + (A_j\cos\theta_j - B_j\sin\theta_j)\sin 2\tau + (A_j\sin\theta_j + B_j\cos\theta_j)\cos 2\tau \tag{A.8}$$

equation (A.7) has steady state solution of the form

$$\begin{aligned}\phi_j^2 &= \lambda_j + E_j\sin 2\tau + F_j\cos 2\tau \\ q_2 &= \nu + G\sin\tau + H\cos\tau.\end{aligned} \tag{A.9}$$

Substitute equation (A.9) into equation (A.7), and separately balance the constant, $\sin\tau$ and $\cos\tau$ terms, to get equations that determine the coefficients $\lambda_j, E_j, F_j, \nu, G$, and H. We need only λ_j for our purposes, so it is sufficient to consider just the constant terms from the top equation:

$$\lambda_j + \frac{1}{2}(B_j\cos\theta_j - A_j\sin\theta_j) = 0. \tag{A.10}$$

Meanwhile, the linear system equations (A.5) and (A.6) are readily solved to give A_j, B_j, with result

$$\begin{pmatrix}A_j\\ B_j\end{pmatrix} = \begin{pmatrix}m_1 & m_2\\ -m_2 & m_1\end{pmatrix}\begin{pmatrix}\sum_\ell\cos\theta_\ell\\ \sum_\ell\sin\theta_\ell\end{pmatrix} + \begin{pmatrix}m_3 & m_4\\ -m_4 & m_3\end{pmatrix}\begin{pmatrix}\cos\theta_j\\ \sin\theta_j\end{pmatrix} \tag{A.11}$$

where

$$\begin{pmatrix} m_1 & m_2 \\ -m_2 & m_1 \end{pmatrix} = \frac{1}{(1+\beta^2)(h^2+g^2)} \begin{pmatrix} -1 & -\beta \\ \beta & -1 \end{pmatrix} \begin{pmatrix} h & g \\ -g & h \end{pmatrix} \begin{pmatrix} 1 & \beta \\ -\beta & 1 \end{pmatrix} \tag{A.12}$$

$$\begin{pmatrix} m_3 & m_4 \\ -m_4 & m_3 \end{pmatrix} = \frac{1}{1+\beta^2} \begin{pmatrix} \beta & -1 \\ 1 & \beta \end{pmatrix} \tag{A.13}$$

with $h = \beta + \left(\Omega^2 - 1\right) \frac{1+\beta^2}{\mu N}$ and $g = 1 + \frac{1+\beta^2}{\mu N}\Gamma$. Combining equations (A.10) and (A.11) one finds, after some algebra,

$$\lambda_j = \frac{1}{2}\left[m_4 - m_1 \sum_\ell \sin\left(\theta_\ell - \theta_j\right) + m_2 \sum_\ell \cos\left(\theta_\ell - \theta_j\right)\right] \tag{A.14}$$

where

$$m_1 = \frac{2\beta g + \left(\beta^2 - 1\right) h}{(1+\beta^2)(h^2+g^2)} \tag{A.15}$$

$$m_2 = -\frac{2\beta h + \left(1 - \beta^2\right) g}{(1+\beta^2)(h^2+g^2)} \tag{A.16}$$

$$m_4 = -\frac{1}{1+\beta^2}. \tag{A.17}$$

ORCID iDs

Kurt Wiesenfeld https://orcid.org/0000-0002-7758-1005

References

[1] Josephson B D 1962 Possible new effects in superconducting tunneling *Phys. Lett.* **1** 251–3
[2] Feynmann R P, Leighton R B and Sands M 1965 *The Feynmann Lectures in Physics* vol III (Reading, MA: Addison-Wesley) pp 21–14
[3] de Gennes P G 1966 *Superconductivity of Metals and Alloys* (New York: W.A. Benjamin)
[4] Orlando T P and Delin K A 1991 *Foundations of Applied Superconductivity* (Reading, MA: Addison-Wesley)
[5] Stewart W C 1968 *Appl. Phys. Lett.* **12** 277
[6] McCumber D E 1968 *J. Appl. Phys.* **39** 3113
[7] Likharev K K 1986 *Dynamics of Josephson Junctions and Circuits* (New York: Gordon and Breach)
[8] Roberazzi R P and Buhrman R A 1989 *IEEE Trans. Magn.* **25** 1384
[9] Kuramoto Y 1975 Self-entrainment of a population of coupled non-linear oscillators *Proc. Int. Symp. on Mathematical Problems in Theoretical Physics* (*Lecture Notes in Physics* vol 39) ed H Araki (Berlin: Springer) pp 420–2
Kuramoto Y 1984 *Chemical Oscillations, Waves, and Turbulence* (Berlin: Springer)
[10] Sakaguchi H and Kuramoto Y 1986 *Prog. Theor. Phys.* **76** 576
[11] Strogatz S H 1994 Norbert Wiener's brain waves *Frontiers in Mathematical Biology* (*Lecture Notes in Biomathematics* vol 100) (Berlin: Springer)
[12] Wiesenfeld K, Colet P and Strogatz S 1996 Synchronization transitions in a disordered Josephson series array *Phys. Rev. Lett.* **76** 404

Wiesenfeld K, Colet P and Strogatz S 1998 Frequency locking in Josephson arrays: connection with the Kuramoto model *Phys. Rev.* E **57** 1563
[13] Chernikov A A and Schmidt G 1995 Conditions for Synchronization in Josephson-junction arrays *Phys. Rev.* E **52** 3145–9
[14] Belykh V N, Pedersen N F and Soerensen O H 1977 Shunted Josephson-junction model. I. The autonomous case *Phys. Rev.* B **16** 4853–9
[15] Dhamala M and Wiesenfeld K 2002 Generalized stability law for Josephson series arrays *Phys. Lett.* A **292** 269–74
[16] Kautz R (unpublished)
[17] Octavio M, Whan C B and Lobb C 1992 Phase coherence and disorder in Josephson-junction arrays *Appl. Phys. Lett.* **60** 766
[18] Wiesenfeld K, Landsberg A and Filatrella G 1997 Linewidth calculation for bare 2D Josephson arrays *Phys. Lett.* A **233** 373–7
[19] Booi P A A and Benz S P 1994 Emission linewidth measurements of two-dimensional array Josephson oscillators *Appl. Phys. Lett.* **64** 2163–5